International Journal of Pharmaceutics 430 (2012) 372–380

Contents lists available at SciVerse ScienceDirect

International Journal of Pharmaceutics

journal homepage: www.elsevier.com/locate/ijpharm

Enhanced cell uptake of superparamagnetic iron oxide nanoparticles through direct chemisorption of FITC-Tat-PEG$_{600}$-*b*-poly(glycerol monoacrylate)

Chenhong Wang[a], Lei Qiao[a], Quan Zhang[a], Husheng Yan[b,*], Keliang Liu[a,**]

[a] Beijing Institute of Pharmacology and Toxicology, Beijing 100850, China
[b] Key Laboratory of Functional Polymer Materials, Ministry of Education, Institute of Polymer Chemistry, Nankai University, Tianjin 300071, China

ARTICLE INFO

Article history:
Received 26 December 2011
Received in revised form 27 March 2012
Accepted 9 April 2012
Available online 16 April 2012

Keywords:
Superparamagnetic iron oxide (SPIO) nanoparticle
Multifunctional magnetic nanoparticle system
FITC-Tat penetrating peptide

ABSTRACT

Magnetic nanoparticles (MNPs) functionalized with specific ligands are emerging as a highly integrated platform for cancer targeting, drug delivery, and magnetic resonance imaging applications. In this study, we describe a multifunctional magnetic nanoparticle system (FITC-Tat MNPs) consisting of a fluorescently labeled cell penetrating peptide (FITC-Tat peptide), a biocompatible block copolymer PEG$_{600}$-*b*-poly(glycerol monoacrylate) (PEG$_{600}$-*b*-PGA), and a superparamagnetic iron oxide (SPIO) nanoparticle core. The particles were prepared by direct chemisorption of PEG$_{600}$-*b*-PGA conjugated with FITC-Tat peptide on the SPIO nanoparticles. FITC-MNPs without Tat were prepared for comparison. Flow cytometry assays revealed significantly higher uptake of FITC-Tat MNPs compared to FITC-MNPs in Caco-2 cells. These results were confirmed using confocal laser scanning microscopy (LSCM), which further demonstrated that the FITC-Tat MNPs accumulated in the cytoplasm and nucleus while the FITC-MNPs were localized in the cell membrane compartments. The FITC-Tat MNPs did not exhibit observable cytotoxicity in MTS assays.

1. Introduction

Magnetic resonance imaging (MRI) has become a vital non-invasive tool in clinical oncology due to its superb anatomical and functional images in high spatial and temporal resolution. The image contrast in MRI relies on the relaxation properties of water protons in the presence of strong external magnetic fields. The quality of the image may be improved through the use of contrast-enhancing agents to help distinguish malignancies from normal tissue (Khemtong et al., 2009; Rai et al., 2010). Superparamagnetic iron oxide (SPIO) nanoparticles (usually composed of Fe_2O_3 and Fe_3O_4) between 3 and 10 nm in size have received considerable attention due to their remarkable magnetic properties and low toxicity.

SPIO nanoparticles are not only an excellent contrast-enhancing agent in MRI, but may also function as carriers in targeted drug delivery systems, being directed to the desired sites by external magnetic fields (Mudry et al., 2003). However, the cell and nuclear membranes act as barriers to most available SPIO nanoparticles, which are not actively translocated into cells and are predominantly restricted to the extracellular space (Fuente and Berry, 2005). The nanoparticles may be functionalized with specific ligands for improving cellular and nuclear uptake. One approach is to attach a ligand such as folate (Pradhan et al., 2010; Yang et al., 2008), transferrin (Yallapu et al., 2010), RGD tripeptide (Huang et al., 2009; Montet et al., 2006), or monoclonal antibodies (Toma et al., 2005) to target a corresponding receptor on the tumor cell surface. It has been clearly established that active targeting results in greater accumulation of nanoparticles in tumors. Most drug delivery systems rely on the receptor-mediated endocytotic pathway for internalization into cells. This pathway leads to the entrapment and, to a large extent, degradation of transported biomolecules in lysosomes (Sethuraman and Bae, 2007).

Another promising approach is to use cell-penetrating peptides (CPPs), which have the advantage of avoiding this pathway and delivering the payload directly into cells. CPPs are a family of proteins defined by the presence of a domain conferring the ability to cross the plasma membrane. Among the large variety of CPPs available, Tat peptide derived from the HIV-1 Tat protein has been the most intensively studied and carries a transmembrane and a nuclear localization signal within its sequence (Vivès et al., 1997). Through its membrane translocation function Tat peptide is capable of mediating intracellular delivery of many different materials including proteins (Bidwell et al., 2009), micelles (Xiong et al.,

* Corresponding author. Tel.: +86 22 23503509; fax: +86 22 23503510.
** Corresponding author. Tel.: +86 10 68169363; fax: +86 10 68211656.
E-mail addresses: yanhs@nankai.edu.cn (H. Yan), keliangliu55@126.com, keliangliu@yahoo.com (K. Liu).

0378-5173/$ – see front matter © 2012 Elsevier B.V. All rights reserved.
http://dx.doi.org/10.1016/j.ijpharm.2012.04.035

2010), oligonucleotides (Lebleu et al., 2008), plasmid DNA (Song et al., 2010; Yang et al., 2009), liposomes (Trabulo et al., 2008), nanoparticles (Rao et al., 2008), and imaging and radiotherapeutic agents (Juliano et al., 2009).

The synthesis of modified magnetic nanoparticles involves a series of chemical processes. The magnetic nanoparticles are formed and then functionalized with various biomaterials, targeting ligands, cell penetrating peptides, or drug molecules depending on the application. An excess of reactants and catalysts is generally required to drive the chemical reaction during the surface modification (Veiseh et al., 2010), and it is therefore difficult to adjust the properties of the MNP surface in a reproducible manner. MNPs prepared using this post-functionalization method may have significant batch-to-batch variations in their physical, chemical, and biological properties (Gu et al., 2008). In addition, surface functionalization with macromolecules is usually difficult due to steric hindrance.

We have developed a novel synthetic method in which multifunctional magnetic nanoparticles are produced through self-assembly of pre-functionalized biomaterials. This method results in precisely engineered NPs produced using simple conjugation and purification procedures that are amenable to scale-up with little batch-to-batch variability. In addition, the ability to precisely engineer targeted NPs may enable the formulation of NPs with slight variations, making it possible to optimize their properties through a combinatorial approach (Gu et al., 2008).

In our previous work, poly(glycerol monoacrylate) replaced ClO_4^- on the surface of the as-synthesized SPIO nanoparticles through direct chemisorption. We also prepared folate-tetra(ethylene glycol)-poly(glycerol monoacrylate) (FA-TEG-PGA) coated Fe_3O_4 nanoparticles that possess excellent stability over a wide range of pH and salt concentrations (Zhang et al., 2009). In the current study, we prepared the functional block polymer FITC-Tat-PEG_{600}-*b*-PGA, and FITC-Tat magnetic nanoparticles were produced through self-assembly of FITC-Tat-PEG_{600}-*b*-PGA and iron oxide-based magnetic nanoparticles. We hypothesized that FITC-Tat MNPs would provide a platform for high-efficiency drug delivery due to the combination of magnetic field-enhanced cell surface accumulation of magnetic nanoparticles and Tat peptide-mediated membrane transport. In order to quantify the penetration ability, FITC-labeled magnetic nanoparticles (FITC-MNPs) were also prepared. Initial assays were performed using Caco-2 cells to test the internalization of the magnetic nanoparticles. Cell uptake was measured using fluorescence activated cell sorting (FACS) and fluorescent optical imaging techniques.

2. Materials and methods

2.1. Materials and general characterization

N-maleimido-functionalized PEG_{600}-*b*-PGA was prepared in our lab (M_n: 5.5×10^3, measured using GPC). Peptides and conjugates were analyzed using RP-HPLC with a linear gradient and a flow rate of 1.0 mL/min, in a mobile phase consisting of (A) 0.1% aqueous trifluoroacetic acid (TFA) and (B) 0.1% TFA in 70% aqueous acetonitrile (ACN). The fractions were analyzed using a Shimadzu LC-10AT VP Plus liquid chromatograph and SPD-10A VP Plus UV–vis detector operating at 210 nm and equipped with a WondaSil™ (C18, 5 μm, 4.6 × 150 mm GL Sciences, Japan) reverse-phase column. Matrix-assisted laser desorption/ionization time-of-flight (MALDI-TOF) mass spectra were recorded on a Bruker Reflex mass spectrometer (Bruker Daltonics, Inc. USA) in positive electrospray mode using α-cyano-4-hydroxycinnamic acid as the matrix and a mixture of $TFA/CH_3CN/H_2O$ as the solvent. Gel permeation chromatography (GPC) was performed using a Waters 515 HPLC pump, a Waters 2414 refractive index detector, and three Styragel columns (HT-2, HT-3, and HT-4). Linear polystyrene standards were used as calibration samples. The eluent was anhydrous THF and the flow rate was l.0 mL/min. ^{1}H-NMR spectra were recorded on a JNM-ECA-400 spectrometer with deuterated solvents at room temperature. The UV–vis absorbance was measured using a UV-2550 detector (Shimadzu, Japan).

2.2. Preparation of superamagnetic nanoparticles

2.2.1. Synthesis of FITC labeled Tat-derived peptide

The Tat-derived peptide (ω-Ahex)-GCGGG*YGRKKRRQRRR* (the italicized amino acids correspond to residues 48–57 of the Tat protein) was synthesized using the conventional Fmoc protocol with 2-(^{1}H-benzotriazole-1-yl)-s1,1,3,3-tetramethyluronium hexafluorophosphate (HBTU) and hydroxybenzotriazole (HOBt) as activating agents in a microwave peptide synthesizer (Liberty, CEM Corporation, USA). Fmoc-Arg(Pbf) was anchored to 0.1 mmol of Rink amide MBHA resin (0.8 mmol/g, Nankai Hecheng, China) and followed with other amino acids purchased from Chengnuo Ind. (China), e.g., Fmoc-Arg(Pbf), Fmoc-Gln(Trt), Fmoc-Lys(Boc), Fmoc-Gly, Fmoc-Tyr(tBu) and Fmoc-Cys(Trt). Fmoc-ω-Aminohexanoic acid (Fmoc-ω-Ahex) was synthesized according to the procedure in reference (Carpino and Han, 1972). The N-terminal was capped with Fmoc-ω-Ahex and the deprotected amino group was treated with 0.4 mmol of fluorescein isothiocyanate (FITC) (AMERSCO, USA) in 5 mL of diisopropylethylamine (DIEA)/DMF (20% v/v) overnight. The reaction was verified by a negative ninhydrin reaction, and the desired peptide FITC-(ω-Ahex)-GCGGG*YGRKKRRQRRR* was cleaved using 10 mL of TFA/thioanisole/ethandithiol/anisole (90/5/3/2) for 3 h at room temperature and precipitated by adding cold ether (−20 °C). The precipitate was filtered and washed with 3 × 20 mL portions of cold ether and the peptide was dissolved in DI water and lyophilized. Crude peptides were purified using C18 reversed-phase HPLC. MALDI-TOF $(M+H)^+$: 2392 (calc.), 2391 (found).

2.2.2. FITC-Tat-PEG_{600}-b-PGA synthesis

A 2.0×10^{-5} mol sample of *N*-maleimido-functionalized PEG_{600}-*b*-PGA (M_n: 5.5×10^3 by GPC) and 4.0×10^{-5} mol of crude FITC-(ω-Ahex)-GCGGG*YGRKKRRQRRR* were dissolved in 5 mL of DI water. The mixture was stirred at room temperature and the reaction was monitored using HPLC. After the reaction was completed, the unreacted peptide was removed by placing the mixture in dialysis tubing (MWCO 3500) and dialyzing 4 times against water over 48 h (Spectra/Por, Laguna Hills, CA). A yellow polymer was obtained after freeze-drying. A ^{1}H NMR peak at 6.69 ppm assigned to the double bonds of the maleimido group disappeared following the reaction.

2.2.3. FITC-(ω-Ahex)-Cys-PEG_{600}-b-PGA synthesis

The peptide FITC-(ω-Ahex)-Cys was synthesized using a manual solid-phase procedure. A 0.1 mmol of Rink amide MBHA resin (0.8 mmol/g, Nankai Hecheng, China) was swelled in CH_2Cl_2. After deprotection of the Fmoc group in the resin, Fmoc-Cys(Trt) and Fmoc-ω-Ahex were anchored to the resin in succession using DCC/HOBt coupling chemistry. FITC was conjugated using the same method described above. Every step of the reaction was verified by a negative ninhydrin test. The peptide was cleaved and precipitated using the same method described above. The precipitate was collected by filtration and washed with 3 × 20 mL portions of cold ether. Due to the lower solubility in water, the peptide was dissolved in acetonitrile and dried by evacuation. The purity of the crude peptide was 90% measured using C18 reversed-phase HPLC. MALDI-MS $(M+H)^+$: 622 (calc.), 623 (found). The synthetic procedure for FITC-(ω-Ahex)-Cys-PEG_{600}-*b*-PGA was the same as that of

FITC-Tat-PEG_{600}-*b*-PGA. A yellow polymer was obtained following dialysis and freeze-drying.

2.2.4. Preparation of FITC-MNP and FITC-Tat MNP

$HClO_4$-stabilized Fe_3O_4 magnetic nanoparticles were prepared according to our previously described method (Zhang et al., 2009). The final particle concentration was 32 mg mL^{-1}, which was determined by evaporating ~2 mL of the colloid to dryness.

A 100 mg sample of the block polymer (FITC-Tat-PEG_{600}-*b*-PGA or FITC-(ω-Ahex)-Cys-PEG_{600}-*b*-PGA) was dissolved in 5 mL of DI water and 200 μL of $HClO_4$-stabilized Fe_3O_4 magnetic nanoparticles were added. The mixture was stirred under Ar for 24 h then centrifuged (15,000 × *g* RCF, 20 min) to sediment the nanoparticles. After removing the supernatant, the sediment could be easily redispersed in DI water by shaking or sonication. The sedimentation and redispersion cycle was repeated three times to remove any remaining polymer. The final nanoparticles were redispersed in DI water. The same experiment was repeated 3 times.

2.3. Determination of Tat peptide content in FITC-Tat-PEG_{600}-b-PGA and FITC-Tat MNPs

Ultraviolet (UV) absorbance spectroscopy was used to determine the amount of FITC-Tat peptide derivative immobilized on the magnetic nanoparticle surface. The yields of Tat conjugation were determined from the UV intensity of the polymer and nanoparticles dissolved in DI water based upon a calibration curve constructed using FITC-Tat peptide at 497 nm. The FITC content of the FITC-MNPs was measured using the same method.

2.4. Determination of Fe_3O_4 content in FITC-Tat MNPs and FITC-MNPs

The Fe_3O_4 content of the FITC-Tat MNPs was measured using the phenanthroline spectrophotometric method. FITC-Tat MNP powder (~5 mg) was placed in a flask and concentrated HCl (1.0 mL) was added. The mixture was heated to 60 °C for 2.5 h with stirring. The yellow solution was diluted to 50 mL with water and a 1 mL aliquot was combined with aqueous solutions of hydroxylamine hydrochloride (1.0 wt%, 0.5 mL) and sodium acetate (1.0 mol L^{-1}, 1 mL). After 2 min, 0.1 mL of 0.1% ortho-phenanthroline was added and the solution was diluted to 10 mL. The absorbance at 510 nm was measured and the Fe content was determined based on comparison to a standard curve. The Fe_3O_4 content of the FITC-Tat MNPs was calculated from the Fe content. The Fe_3O_4 content of the FITC-MNPs was calculated using the same method.

2.5. Thermogravimetric analysis

Thermogravimetric analysis (TGA) was carried out on powder samples (~10 mg) using a TA Instruments SDT Q600 V8.2 Build 100, ramping from 25.00 to 100.00 °C at a heating rate of 20.00 °C/min, holding for 15.00 min, then heating at 10.00 °C/min to 815.00 °C under N_2 flow.

2.6. Determination of mean diameters and ζ potential of FITC-Tat MNPs and FITC-MNPs

Both measurements were performed at 25 °C using a Malvern Zetasizer NanoZS90 instrument equipped with a 633 nm laser at a fixed scattering angle of 90°. The magnetic nanoparticles were dispersed in DI water from a Milli-Q® ultra-pure water system and the concentration was approximately 1 mg mL^{-1}. The samples were measured without filtration. The reported values are the averages of five measurements.

2.7. Stability of Tat peptide in FITC-Tat MNPs

The Tat peptide stability in the FITC-Tat-PEG_{600}-*b*-PGA and FITC-Tat MNPs was investigated by incubation with 10 μg mL^{-1} trypsin, 10 μg mL^{-1} chymotrypsin, and 10 mmol L^{-1} DTT in PBS solution at 37 °C for 24 h. The solution was centrifuged (14,000 × *g* RCF, 10 min) in an Amicon® Ultra-0.5 mL, 3 KDa Centrifugal Filter Unit (Millipore, USA) and the filtrate was examined using a UV–vis spectrophotometer.

2.8. Study on the transport of FITC-Tat MNPs by FACS

2.8.1. Cell culture

Caco-2 cells were purchased from ATCC (Manassas, VA, USA). Cells were cultured in DMEM (Dulbecco's modified Eagles Medium) with glucose (4.5 mg mL^{-1}) containing 20% fetal bovine serum (FBS) for the first two passages after thawing, and 10% FBS for further maintenance. The medium was supplemented with penicillin (100 U mL^{-1}), streptomycin (100 mg mL^{-1}), Na-pyruvate (1 mmol L^{-1}), L-glutamine (2 mmol L^{-1}), and nonessential amino acids (0.1 mmol L^{-1}), which were purchased from HyClone (HyClone Laboratories Inc, South Logan, Utah, USA). Cells were cultured according to standard conditions, and passages 20–30 were used.

2.8.2. Cellular uptake kinetics assay

Caco-2 cells grown as a monolayer were harvested with 0.25% (w/v) trypsin – 0.02% (w/v) EDTA solution and were seeded in 12 well plates at a density of 2.5×10^5 cells per well and incubated for 24 h. Test samples of FITC-Tat MNPs and FITC-MNPs possessing the same UV absorption at 497 nm were added to the wells and incubated for 1 h, 2 h, 3 h, or 4 h. After incubation, the cells were washed with HBSS (4×) and trypsinized for 5 min. Trypsinization was halted by addition of cold DMEM containing 10% FCS. Cells were separated by pipetting up and down several times, transferred to FACS tubes (Becton Dickinson), and centrifuged. Cells were analyzed on a FacsCalibur (Becton Dickinson, Franklin Lakes, NJ, USA). The excitation wavelength was 488 nm and the fluorescence was measured with the FL1 channel. A total of 10,000 cells per sample were analyzed. The number of cells with fluorescence intensity was used to determine the fraction of labeled cells. The baseline was obtained by analyzing unlabeled control cells. The relative median fluorescence was calculated by dividing the median of the labeled cells by the median of an unlabeled cell population.

2.8.3. Cellular uptake of FITC-Tat MNPs at various concentrations

Caco-2 cells grown as a monolayer were harvested with 0.25% (w/v) trypsin – 0.02% (w/v) EDTA solution and seeded in 12 well plates at a density of 2.5×10^5 cells per well and incubated for 24 h. Several concentrations (from 0.1 mg mL^{-1} to 1.0 mg mL^{-1}) of FITC-Tat MNPs were added to the wells and incubated for 4 h. The cells were harvested and the fluorescence was measured using FACS.

2.8.4. Cellular uptake of FITC-Tat MNP in a magnetic field

Caco-2 cells grown as a monolayer and harvested with 0.25% (w/v) trypsin – 0.02% (w/v) EDTA solution were seeded in 35 mm culture dishes (Corning, Inc., Corning, NY) at a density of 5×10^4 cells mL^{-1} and incubated for 24 h. The cells were washed with PBS and each dish was incubated with 1.5 mL FITC-Tat MNP/PBS solution (corresponding to 20 μg mL^{-1} Fe) for 15 min. During the process, an 18 × 5 mm cylindrical sintered Nd–Fe–B magnet (remanence Br, 1080–1150 mT; Ruifeng magnet, Beijing, China) was placed under one of the dishes. The cells were harvested and the fluorescence was measured using FACS.

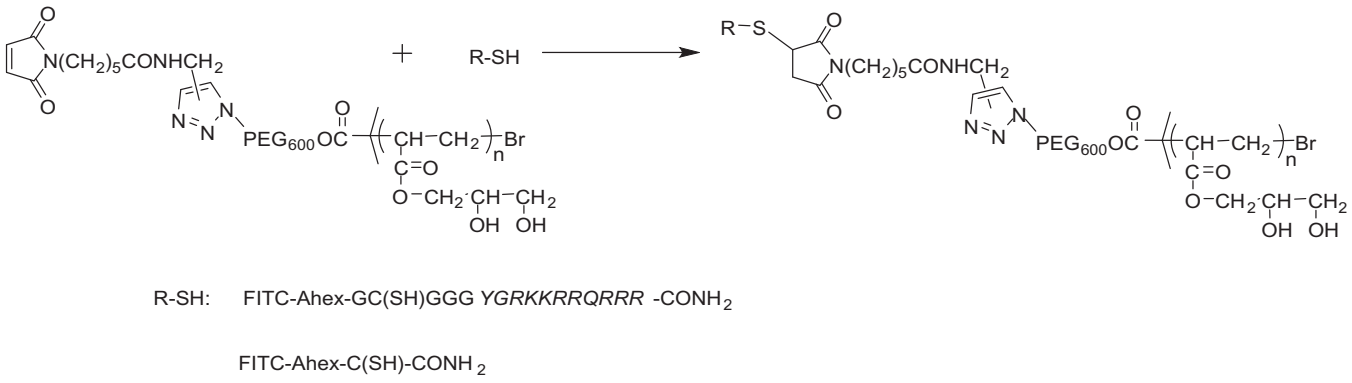

Scheme 1. Synthesis of FITC-Tat-PEG$_{600}$-*b*-PGA and FITC-(ω-Ahex)-Cys-PEG$_{600}$-*b*-PGA.

2.9. Study on the transport of FITC-Tat MNPs by confocal microscopy

Caco-2 cells were seeded at a concentration of 5×10^4 cells mL^{-1} in 35 mm glass bottom culture dishes (Mat-Tek corporation, Ashland, U.S.A.) with glass cover slips and grown for 24 h. The cells were incubated for 2 h in complete media containing FITC-Tat MNPs or FITC-MNPs and washed three times with PBS. The cells were fixed in phosphate-buffered saline (PBS) – 4% formaldehyde for 10 min and incubated in RNase A (1 μg mL^{-1}, Sigma) for 30 min, permeabilized with 0.1% Triton X-100 (Sigma) for 5 min at room temperature, and stained with PI (3 μg mL^{-1}, Sigma) for 30 min. After washing three times with PBS, the cells were examined using a Carl Zeiss LSM 510 meta fluorescence microscope with long focal length optics and excitation using green He–Ne (543 nm) and argon ion (488 nm) lasers.

2.10. Study on the cytotoxicity of the FITC-Tat MNPs by MTS assay

Caco-2 cells were seeded in 96-well cell culture plates (Corning, Inc., Corning, NY) at a density of approximately 1×10^4 cells per well in DMEM supplemented with 10% (v/v) FCS and incubated for 48 h. The cells were washed twice with HBSS and incubated with 100 μL of nanoparticle suspension at the indicated concentration at 37 °C for 24 h. The cells were washed with HBSS to remove the nanoparticles and re-suspended in 80 μL HBSS. Thereafter, 20 μL of Cell Titer 96® AQueous One Solution Reagent (Promega Corp, Madison, WI, USA) was added to each well, followed by an incubation period of 2 h. The solution absorbance was measured at 490 nm using a SpectraMax® M5 (Molecular Devices). HBSS was used as a negative control. Cell viability data were obtained by calculating the ratio of viable cells in the treated cultures to the untreated control cells. The experiment was repeated 5 times for each nanoparticle concentration.

3. Results and discussion

3.1. Conjugation of polymer and fluorescent peptide

The reaction between the maleimido and sulfhydryl groups is specific (Scheme 1) and the *N*-maleimido-functionalized PEG$_{600}$-*b*-PGA reacted with the FITC-Tat peptide very quickly (Fig. 1). The red and black lines represent the starting concentrations of *N*-maleimido-functionalized PEG$_{600}$-*b*-PGA and FITC-Tat peptide. The green line depicts the spectrum after 5 min reaction. The peak height corresponding to the FITC-Tat peptide decreased, and the product peak from FITC-Tat-PEG$_{600}$-*b*-PGA was clearly shifted to the right (lower polarity). After dialyzation to remove the excess FITC-Tat peptide, ^{1}H NMR (Fig. 2) analysis revealed the

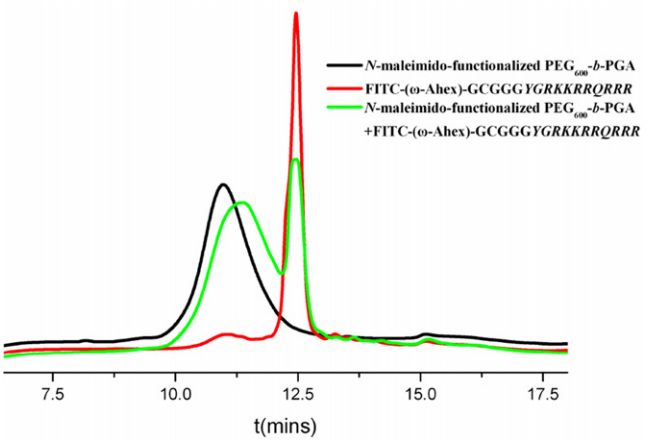

Fig. 1. HPLC chromatograms of *N*-maleimido-functionalized PEG$_{600}$-*b*-PGA (black line), FITC-(ω-Ahex)-GCGGG*YGRKKRRQRRR* (red line), and *N*-maleimido-functionalized PEG$_{600}$-*b*-PGA + FITC-(ω-Ahex)-GCGGG*YGRKKRRQRRR* (green line). (For interpretation of the references to color in this figure legend, the reader is referred to the web version of the article.)

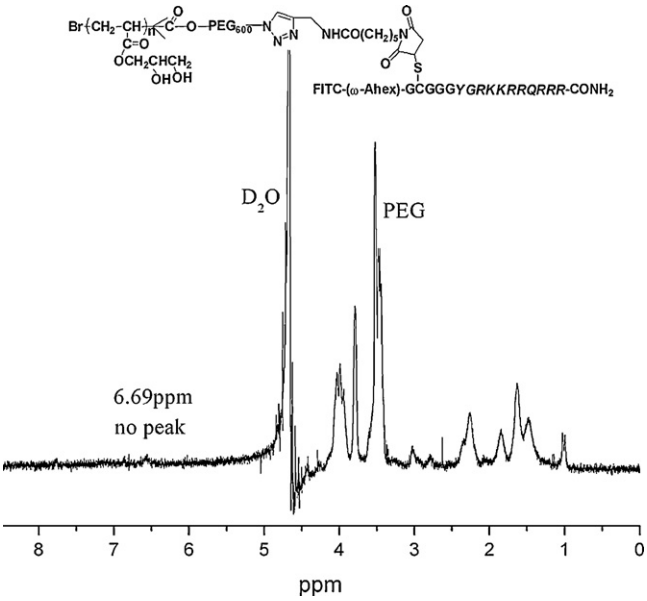

Fig. 2. ^{1}H NMR spectrum of FITC-Tat-PEG$_{600}$-*b*-PGA.

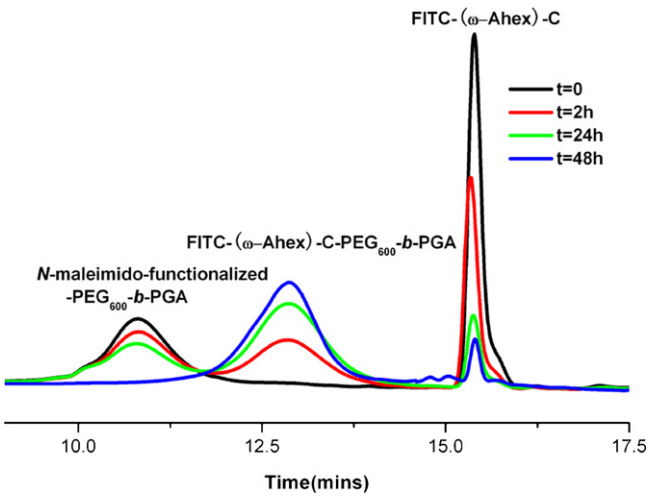

Fig. 3. HPLC chromatograms describing course of reaction of *N*-maleimido-functionalized PEG_{600}-*b*-PGA with FITC-(ω-Ahex)-Cys.

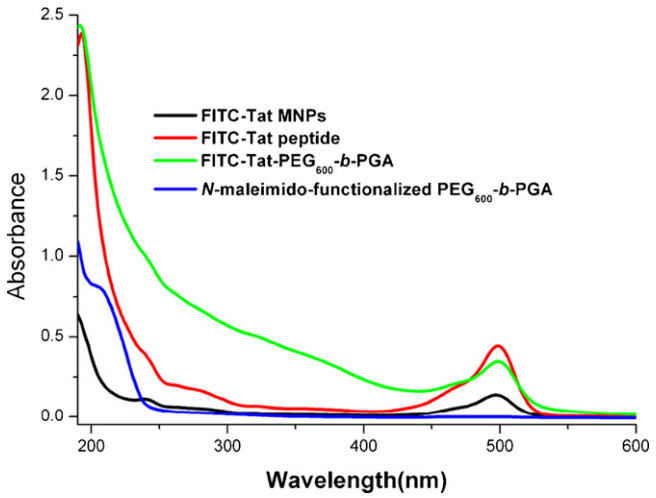

Fig. 5. Absorption spectra of FITC-Tat derivatives and magnetic nanoparticles. (For interpretation of the references to color in this figure legend, the reader is referred to the web version of the article.)

disappearance of the maleimido group (6.69 ppm) peak in the product polymer, indicating that the *N*-maleimido-functionalized PEG_{600}-*b*-PGA was completely consumed.

For comparison, FITC-coupled magnetic nanoparticles lacking the Tat peptide (i.e., FITC-(ω-Ahex)-Cys-PEG_{600}-*b*-PGA) were prepared by coupling FITC-(ω-Ahex)-Cys with *N*-maleimido-functionalized PEG_{600}-*b*-PGA. HPLC analysis (Fig. 3) indicated that the coupling rate was slower than when using FITC-Tat peptide (Fig. 1). This may be attributed to the lower solubility of FITC-(ω-Ahex)-Cys in water.

3.2. Determination of number of FITC-Tat peptides in FITC-Tat MNPs and FITC in FITC-MNPs

FITC-Tat MNPs were obtained by chemisorption of FITC-Tat-PEG_{600}-*b*-PGA on the surface of $HClO_4$-stabilized Fe_3O_4 nanoparticles (Fig. 4). FITC-MNPs were prepared in the same manner.

Fig. 5 contains typical UV–vis absorption spectra of *N*-maleimido-functionalized PEG_{600}-*b*-PGA (blue line), FITC-Tat peptide (red line), FITC-Tat-PEG_{600}-*b*-PGA (green line), and FITC-Tat MNPs (black line). The peak at 497 nm from FITC was observed in FITC-Tat peptide, FITC-Tat-PEG_{600}-*b*-PGA, and FITC-Tat MNPs, indicating that FITC-Tat-PEG_{600}-*b*-PGA was successfully incorporated in the MNPs, and UV spectroscopy could be used to determine the number of tat peptides associated with the nanoparticles due to the special absorption of FITC. The FITC-MNPs were also characterized using UV–vis absorption spectroscopy (Fig. 6). The number of FITC-Tat-PEG_{600}-*b*-PGA and FITC-(ω-Ahex)-Cys-PEG_{600}-*b*-PGA-stabilized nanoparticles could be determined from the UV spectra.

The TGA curves of $HClO_4$ MNPs, FITC-Tat MNPs, and FITC-Tat-PEG_{600}-*b*-PGA were measured in a nitrogen atmosphere and are displayed in Fig. 7. FITC-Tat MNPs and FITC-Tat-PEG_{600}-*b*-PGA are very hygroscopic due to the large number of hydroxyl groups in PGA, and adsorbed water was removed by heating from 25 to 100 °C and holding at this temperature for 15.00 min. The weight losses of FITC-Tat MNPs and FITC-Tat-PEG_{600}-*b*-PGA were both less than 5% below 100 °C. The weight loss of $HClO_4$ MNP was approximately 5.02% over the entire temperature range, largely due to removal of $HClO_4$. FITC-Tat-PEG_{600}-*b*-PGA and FITC-Tat MNPs exhibited significant weight loss because low molecular weight PEG degrades at ~280 °C (Granqvist and Buhrman, 1976). When the temperature reached 500 °C, FITC-Tat-PEG_{600}-*b*-PGA was completely decomposed and no further weight loss occurred at higher temperatures. The same behavior was observed in FITC-Tat MNPs. When the temperature reached 750 °C, the residual mass of the

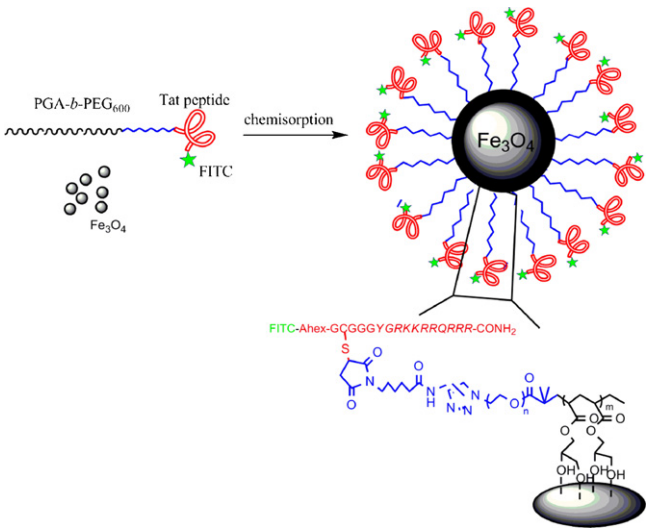

Fig. 4. Schematic of preparation of FITC-Tat MNPs.

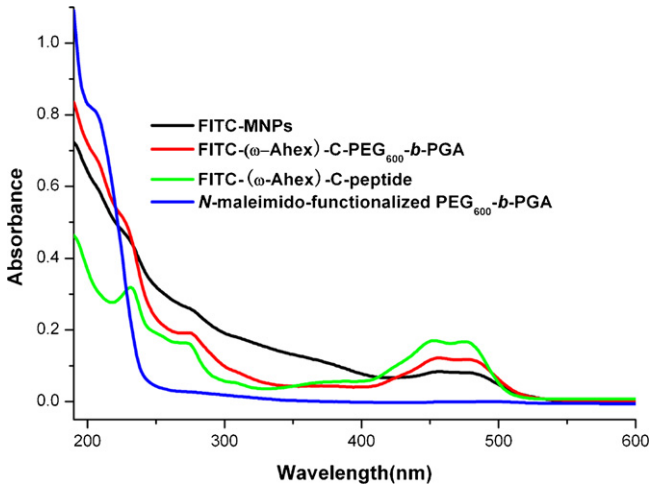

Fig. 6. Absorption spectra of FITC labeled derivatives and magnetic nanoparticles.

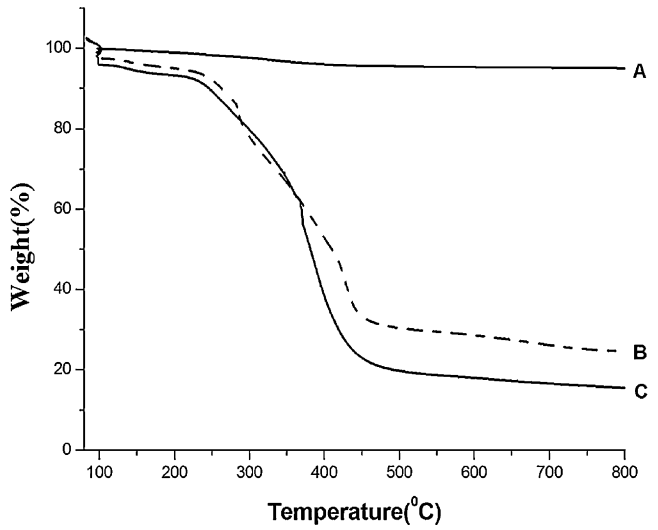

Fig. 7. TGA curves of (A) $HClO_4$ MNPs, (B) FITC-Tat MNPs, (C) FITC-Tat-PEG_{600}-*b*-PGA.

FITC-Tat MNPs was 22.40 wt%, greater than the Fe_3O_4 content (9.66 wt%) determined using the phenanthroline method. This indicates incomplete vaporization of the organic material under a N_2 atmosphere. For comparison, the residual mass of FITC-Tat-PEG_{600}-*b*-PGA was 12.87 wt% at 750 °C. The Fe_3O_4 content obtained from the difference between the residual mass percentages of FITC-Tat-PEG_{600}-*b*-PGA and FITC-Tat MNPs was 9.77 wt%, which was consistent with the value determined using the phenanthroline method. The second weight loss step from 550 to 750 °C was not as obvious, possibly due to the lower Fe_3O_4 content in the FITC-Tat MNPs (Zhang et al., 2009). The Fe_3O_4 content of the FITC-MNPs was 9.29 wt%.

The amounts of Tat peptide in the polymer and nanoparticles were determined from the absorption spectrum. Approximately 80% of the nanoparticle mass consisted of FITC-Tat-PEG_{600}-*b*-PGA conjugate. Based on this and the results of the phenanthroline measurements, the molar ratio of Fe_3O_4 to FITC-Tat peptide was 3.4:1. Assuming that the $HClO_4$-stabilized magnetic nanoparticles used in this study have the inverse spinel structure characteristic of magnetite, a magnetic core with a diameter of 4.6 nm (measured using laser light scattering) theoretically contains 2064 iron atoms (Verwey and Heilmann, 1947). In our experiments the diameter of the Fe_3O_4 nanoparticles was approximately 10 nm based on TEM images. The magnetic cores should therefore contain approximately 21,205 iron atoms and the average number of FITC-Tat peptide molecules per particle is approximately

Table 1
The Fe_3O_4 content and the number of FITC in the FITC-Tat MNPs and FITC-MNPs.

MNPs	Fe_3O_4 content (wt%)[a]	The number of FITC in the MNPs[a]
FITC-Tat MNPs	9.77 ± 1.24	2078 ± 68
FITC-MNPs	9.29 ± 1.68	2192 ± 91

[a] The data were the average of three MNPs.

Table 2
Mean size and ζ potential of FITC-Tat MNPs and FITC-MNPs from DLS measurements.

MNPs	Size (nm)	ζ potential (mv)
FITC-Tat MNPs	65.8 ± 1.7	24.5 ± 3.7
FITC-MNPs	65.3 ± 3.2	−6.0 ± 3.7

2078 (Kohler et al., 2005; Shen et al., 1993). Meantime, the average number of FITC-(ω-Ahex)-Cys in the FITC MNPs is 2192 with the same method (Table 1).

3.3. Determination of size and ζ potential of FITC-Tat MNPs and FITC-MNPs

The size distributions of the FITC-Tat-MNPs and FITC-MNPs were characterized using TEM and DLS. Both of the particle types appeared roughly spherical or ellipsoidal in TEM micrographs. The mean diameter was approximately 10 nm in the images (figure not shown). The average diameters were also determined using DLS and were 65.8 ± 1.7 and 65.3 ± 3.2 nm (Table 2). The larger diameters obtained from DLS measurements reflect the increase in hydrodynamic size resulting from inclusion of FITC-Tat-PEG_{600}-*b*-PGA or FITC-(ω-Ahex)-Cys-PEG_{600}-*b*-PGA (which are not visible in TEM images) (Huang et al., 2009). The ζ potential of the FITC-MNPs was −6.0 ± 3.7 mV. In contrast, the ζ potential of the FITC-Tat MNPs was 24.5 ± 3.7 mV due to the positive charges on the tat peptide.

3.4. Stability of Tat peptide in FITC-Tat MNPs

To verify the stability of FITC-Tat MNPs, the nanoparticle was incubated with trypsin, chymotrypsin, or DTT at 37 °C for 24 h (Wunderbaldinger et al., 2002). None of the treatments resulted in an absorbance peak corresponding to FITC in the filtrate (Fig. 8), indicating that Tat peptide was not removed from the nanoparticles during treatment with these agents. The 24 h stability of the FITC-Tat MNPs and FITC MNPs in different pH value (pH 4–10) and salt concentration ([NaCl] = 1–10 wt%) was also investigated respectively. The nanoparticle sizes from DLS did not change and no any FITC absorbance in the filtrate was observed in UV–vis spectrum (the data not shown).

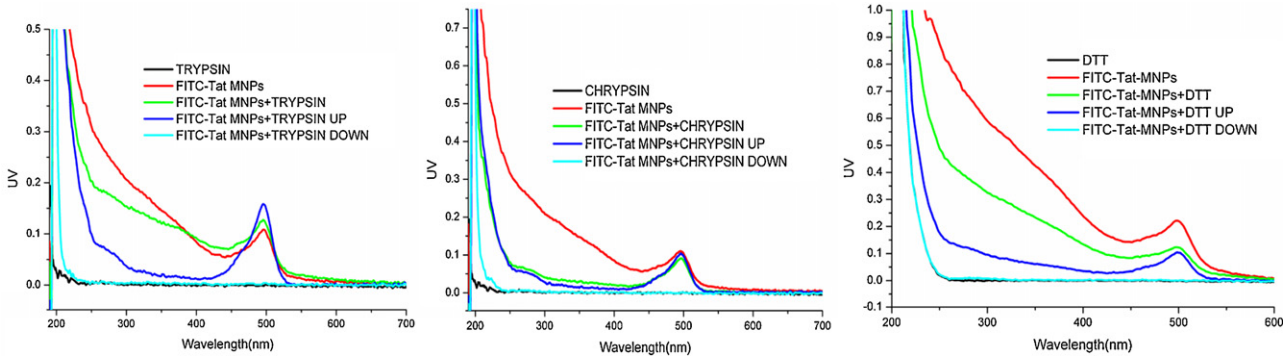

Fig. 8. Absorbance spectra of FITC-Tat MNP suspension after incubation with 10 μg mL^{-1} chymotrypsin, trypsin, or 10 mmol L^{-1} DTT at 37 °C for 24 h.

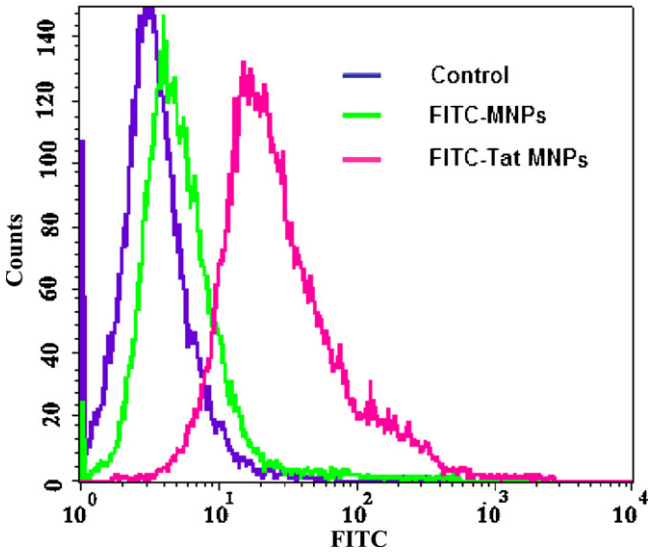

Fig. 9. Cellular uptake of MNPs in Caco-2 cells measured using flow cytometry after 4 h incubation. (Control histogram represents cells incubated in the absence of MNPs.)

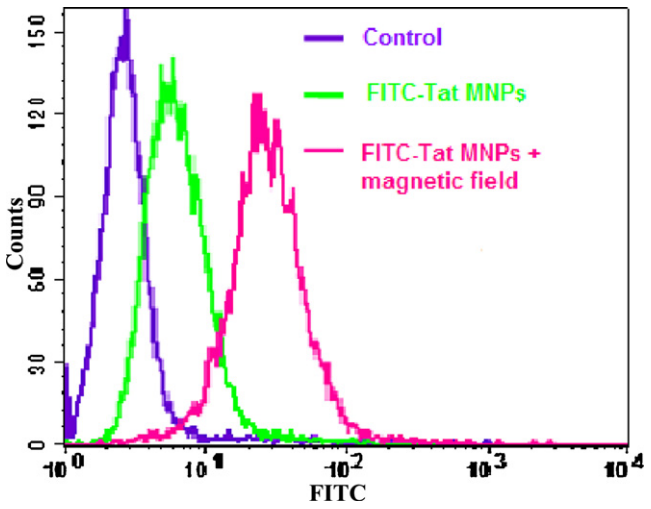

Fig. 11. Cellular uptake of FITC-Tat MNPs in Caco-2 cells after 15 min incubation in magnetic field. (Control histograms represent cells incubated in the absence of MNPs.)

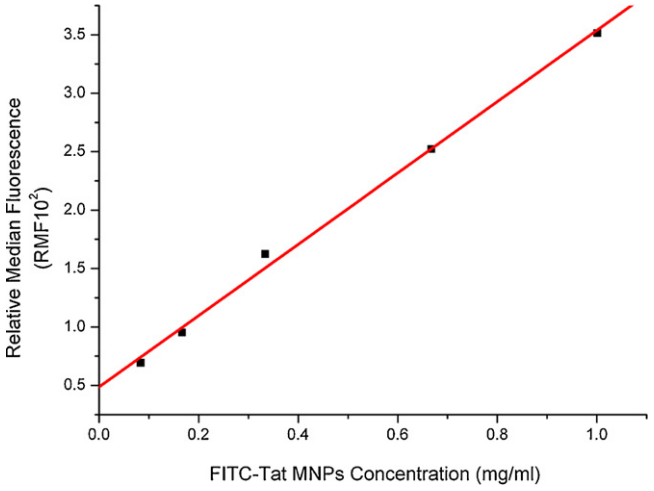

Fig. 10. Uptake of FITC-Tat MNPs by Caco-2 cells after 4 h incubation as function of concentration.

3.5. Penetrating ability of FITC-Tat MNPs in Caco-2 cell

The penetrating ability of MNPs was determined from flow cytometric measurements of fluorescence intensity in Caco-2 cells incubated with FITC-Tat MNPs or FITC-MNPs containing identical amounts of conjugated FITC. Flow cytometry data obtained after 4 h of incubation is provided in Fig. 9. The FITC-Tat MNPs quickly entered the cells, and cells incubated with FITC-Tat MNPs displayed substantially greater fluorescence than those incubated with FITC-MNPs, which exhibited fluorescence almost identical to the control cells. The area under each curve is proportional to the total number of fluorescent cells and was approximately 20 times higher in FITC-Tat MNPs. This indicates that the addition of Tat peptide to the nanoparticles enhances the uptake of the nanoparticles.

The cell uptake of FITC-Tat MNPs was investigated at several concentrations. Interestingly, the relative median fluorescence intensity was linear with respect to FITC-Tat MNP concentration (Fig. 10).

To evaluate the influence of magnetic fields on the cellular uptake of FITC-Tat MNPs, the cells were incubated with FITC-Tat MNPs for 15 min either with or without an applied magnetic field. The field intensity and incubation time were chosen based on previous reports (Scherer et al., 2002). The magnetic field resulted in fluorescence readings almost 5 times higher (Fig. 11). The enhanced cell uptake may be due to an increase in nanoparticle concentration near the cell surface.

Although flow cytometry results are more quantitative than confocal microscopy images, they do not identify the actual location of the MNPs. Caco-2 cells were incubated for 2 h with fluorescent magnetic nanoparticles (FITC-Tat MNP or FITC-MNP) and examined using laser scanning confocal microscopy (LSCM). Fig. 12 contains a series of micrographs employing various stains. In order to determine the location of the nanoparticles inside the cells, the cell profile was shown in the bright field; DNA within the cell nuclei was stained with PI. The green color of FITC was scarce and was located almost entirely outside the cell membrane (Fig. 12A), suggesting that FITC-MNPs do not penetrate the cell membrane. In contrast, a yellow color resulting from combination of green and red observed in Fig. 12B, indicating that the FITC-Tat MNPs were located at the cell nucleus. Green regions were also coincident with the cell profile, suggesting that inclusion of tat peptide enables particles to penetrate the cell membrane and nuclear pores (Sethuraman and Bae, 2007).

3.6. Cytotoxicity of FITC-Tat MNPs

An MTS assay using the Caco-2 cell line was performed to analyze the toxicity of FITC-Tat MNPs and FITC-MNPs (Fig. 13). FITC-Tat MNPs and FITC-MNPs at concentrations ranging from 0.04 to 2.10 mg mL^{-1} were incubated with Caco-2 cells for 24 h. The experiment was repeated 5 times for each concentration. In order to reduce disturbances from nanoparticle absorbance at 490 nm, HBSS was added to one of the five wells in place of MTS solution, and this data was subtracted from the mean value of the other four data points. Fig. 13 reveals that neither FITC-MNPs nor FITC-Tat MNPs displayed significant cytotoxicity (10–15% cell death), even at higher concentrations.

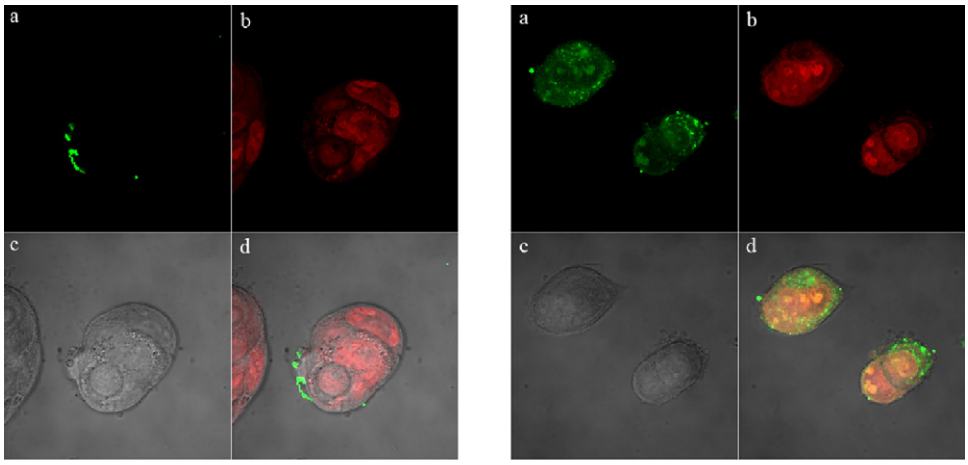

Fig. 12. Laser scanning confocal microscopy (LSCM) images of Caco-2 cells after 2 h incubation with MNPs. (A) FITC-MNPs, (B) FITC-Tat MNPs. Channel (a) MNPs were labeled with FITC. Channel (b) cell nuclei were stained with PI. Channel (c) bright field. Channel (d) mixture of channels a, b, and c. (For interpretation of the references to color in this figure legend, the reader is referred to the web version of the article.)

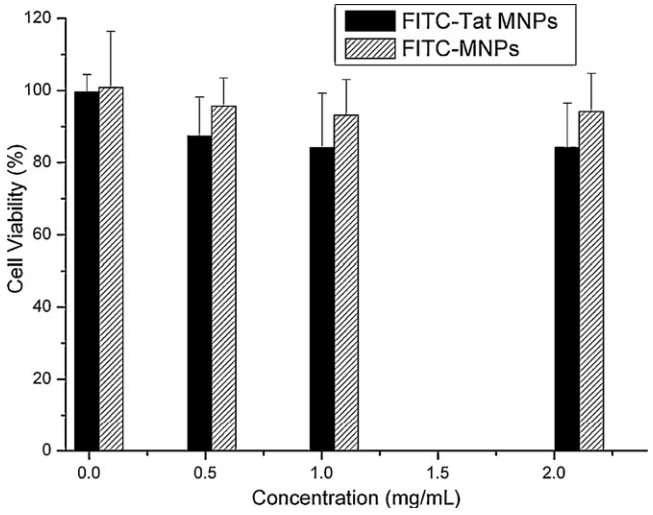

Fig. 13. Cell viability of Caco-2 cells treated with various concentrations of FITC-Tat MNPs or FITC-MNPs measured using the MTS assay. Results are means ± SD ($n = 4$).

4. Conclusion

Multi-functionalized magnetic nanoparticles were prepared by self-assembly of FITC-Tat-PEG$_{600}$-*b*-PGA or FITC-(ω-Ahex)-Cys-PEG$_{600}$-*b*-PGA with superparamagnetic iron oxide. The FITC-Tat MNPs and FITC-MNPs were almost equal in size, while the ζ potential of the FITC-Tat MNPs was significantly higher due to the positive charges on the tat peptide. The amount of FITC-Tat peptide in the SIOP nanoparticle was determined from the UV absorbance of FITC at 497 nm and the Fe content of the nanoparticles. In Caco-2 cells, FITC-Tat MNPs displayed 20-fold greater uptake ability than FITC-MNPs after incubation for 4 h. The uptake speed of FITC-Tat MNPs was proportional to the concentration. In the presence of a magnetic field, the fluorescence intensity due to FITC-Tat MNPs entering the cells increased by a factor of 5. These results were confirmed using LSCM, which further demonstrated FITC-Tat MNPs accumulate in both the cytoplasm and nuclear compartments, while FITC-MNPs remained localized in cell membrane compartments. The FITC-Tat MNPs exhibited low cytotoxicity even at concentrations above 2.0 mg mL^{-1} in MTS assays. These particles may be useful not only in cell imaging, but also in gene therapy and drug delivery.

Acknowledgments

This work was supported by The National Key Technologies R & D Program for New Drugs of China (2009ZX09301-002) and National Natural Science Foundation of China (81001417). The authors wish to thank Dr. Aiping Zheng from the Beijing Institute of Pharmacology & Toxicology for her helpful technical advice in cell culture.

References

Bidwell III, G.L., Davis, A.N., Raucher, D., 2009. Targeting a c-Myc inhibitory polypeptide to specific intracellular compartments using cell penetrating peptides. J. Control. Release 135, 2–10.
Carpino, L.A., Han, G.Y., 1972. 9-Fluorenylmethoxycarbonyl amino-protecting group. J. Org. Chem. 37, 3404–3409.
Fuente, J.M., Berry, C.C., 2005. Tat-peptide as an efficient molecule to translocate gold nanoparticles into cell nucleus. Bioconj. Chem. 16, 1176–1180.
Granqvist, C.G., Buhrman, R.H., 1976. Ultrafine metal particles. J. Appl. Phys. 47, 2200–2220.
Gu, F., Zhang, L.F., Teply, B.A., Mann, N., Wang, A., Radovic-Moreno, A.F., Langer, R., Farokhzad, O.C., 2008. Precise engineering of targeted nanoparticles by using self-assembled biointegrated block copolymers. PNAS 105, 2586–2591.
Huang, G., Zhang, C.F., Li, S.Z., Khemtong, C., Yang, S.G., Tian, R.H., Minna, J.D., Brown, K.C., Gao, J.M., 2009. A novel strategy for surface modification of superparamagnetic iron oxide nanoparticles for lung cancer imaging. J. Mater. Chem. 19, 6367–6372.
Juliano, R.L., Alam, R., Dixit, V., Kang, H.M., 2009. Cell-targeting and cell-penetrating peptides for delivery of therapeutic and imaging agents. WIREs Nanomed. Nanobiotechnol. 1, 324–335.
Khemtong, C., Kessinger, C.W., Gao, J.M., 2009. Polymeric nanomedicine for cancer MR imaging and drug delivery. Chem. Commun. 45, 3497–3510.
Kohler, N., Sun, C., Wang, J., Zhang, M.Q., 2005. Methotrexate-modified superparamagnetic nanoparticles and their intracellular uptake into human cancer cells. Langmuir 21, 8858–8864.
Lebleu, B., Moulton, H.M., Abes, R., Ivanova, G.D., Abes, S., Stein, D.A., Iversen, P.L., Arzumanov, A.A., Gait, M.J., 2008. Cell penetrating peptide conjugates of steric block oligonucleotides. Adv. Drug Deliv. Rev. 60, 517–529.
Montet, X., Funovics, M., Montet-Abou, K., Weissleder, R., Josephson, L., 2006. Multivalent effects of RGD peptides obtained by nanoparticle display. J. Med. Chem. 49, 6087–6093.
Mudry, K.M., Plonsey, R., Bronzino, J., 2003. Biomedical Imaging. CRC Press, Boca Raton.
Pradhan, P., Giri, J., Rieken, F., Koch, C., Mykhaylyk, O., Döblinger, M., Banerjee, R., Bahadur, D., Plank, C., 2010. Targeted temperature sensitive magnetic liposomes for thermo-chemotherapy. J. Control. Release 142, 108–121.
Rai, P., Mallidi, S., Zheng, X., Rahmanzadeh, R., Mir, Y., Elrington, S., Khurshid, A., Hasan, T., 2010. Development and applications of photo-triggered theranostic agents. Adv. Drug Deliv. Rev. 62, 1094–1124.
Rao, K.S., Reddy, M.K., Horning, J.L., Labhasetwar, V., 2008. TAT-conjugated nanoparticles for the CNS delivery of anti-HIV drugs. Biomaterials 29, 4429–4438.

Scherer, F., Anton, M., Schillinger, U., Henke, J., Bergemann, C., Kruger, A., Gansbacher, B., Plank, C., 2002. Magnetofection: enhancing and targeting gene delivery by magnetic force in vitro and in vivo. Gene Ther. 9, 102–109.

Sethuraman, V.A., Bae, Y.H., 2007. TAT peptide-based micelle system for potential active targeting of anti-cancer agents to acidic solid tumors. J. Control. Release 118, 216–224.

Shen, T., Weissleder, R., Papisov, M., Bogdanov, A., Brady, T.J., 1993. Monocrystalline iron oxide nanocompounds (MION): physicochemical properties. Magn. Reson. Med. 29, 599–604.

Song, H.P., Yang, J.Y., Lo, S.L., Wang, Y., Fan, W.M., Tang, X.S., Xue, J.M., Wang, S., 2010. Gene transfer using self-assembled ternary complexes of cationic magnetic nanoparticles, plasmid DNA and cell-penetrating Tat peptide. Biomaterials 31, 769–778.

Toma, A., Otsuji, E., Kuriu, Y., Okamot, K., Ichikawa, D., Hagiwara, A., Ito, H., Nishimura, T., Yamagishi, H., 2005. Monoclonal antibody A7-superparamagnetic iron oxide as contrast agent of MR imaging of rectal carcinoma. Br. J. Cancer 93, 131–136.

Trabulo, S., Mano, M., Faneca, H., Cardoso, A.L., Duarte, S., Henriques, A., Paiva, A., Gomes, P., Simões, S., Lima, M.C.P., 2008. S413-PV cell penetrating peptide and cationic liposomes act synergistically to mediate intracellular delivery of plasmid DNA. J. Gene. Med. 10, 1210–1222.

Veiseh, O., Gunn, J.W., Zhang, M.Q., 2010. Design and fabrication of magnetic nanoparticles for targeted drug delivery and imaging. Adv. Drug Deliv. Rev. 62, 284–304.

Verwey, E.J.W., Heilmann, E.L., 1947. Physical properties and cation arrangement of oxides with spinel structures I. Cation arrangement in spinels. J. Chem. Phys. 15, 174–180.

Vivès, E., Brodin, P., Lebleu, B., 1997. Truncated HIV-1 tat protein basic domain rapidly translocates through the plasma membrane and accumulates in the cell nucleus. J. Biol. Chem. 272, 16010–16017.

Wunderbaldinger, P., Josephson, L., Weissleder, R., 2002. Tat peptide directs enhanced clearance and hepatic permeability of magnetic nanoparticles. Bioconj. Chem. 13, 264–268.

Xiong, X.B., Uludag, H., Lavasanifar, A., 2010. Virus-mimetic polymeric micelles for targeted siRNA delivery. Biomaterials 31, 5886–5893.

Yallapu, M.M., Foy, S.P., Jain, T.K., Labhasetwar, V., 2010. PEG-functionalized magnetic nanoparticles for drug delivery and magnetic resonance imaging applications. Pharm. Res. 27, 2283–2295.

Yang, S., Coles, D.J., Esposito, A., Mitchell, D.J., Toth, I., Minchin, R.F., 2009. Cellular uptake of self-assembled cationic peptide-DNA complexes: multifunctional role of the enhancer chloroquine. J. Control. Release 135, 159–165.

Yang, X.Q., Chen, Y.H., Yuan, R.X., Chen, G.H., Blanco, E., Gao, J.M., Shuai, X.T., 2008. Folate-encoded and Fe_3O_4-loaded polymeric micelles for dual targeting of cancer cells. Polymer 49, 3477–3485.

Zhang, Q., Wang, C.H., Qiao, L., Yan, H.S., Liu, K.L., 2009. Superparamagnetic iron oxide nanoparticles coated with a folate-conjugated polymer. J. Mater. Chem. 19, 8393–8402.